Journal of Biomechanics 92 (2019) 67–75

Contents lists available at ScienceDirect

Journal of Biomechanics

journal homepage: www.elsevier.com/locate/jbiomech
www.JBiomech.com

A geometry-based model for non-invasive estimation of pressure gradients over iliac artery stenoses

S.G.H. Heinen [a,b,*], D.A.F. van den Heuvel [a], J.P.P.M. de Vries [c], F.N. van de Vosse [d], T. Delhaas [b], W. Huberts [b]

[a] Department of Radiology, St. Antonius Hospital, Nieuwegein, the Netherlands
[b] Department of Biomedical Engineering, CARIM School for Cardiovascular Diseases Maastricht University Medical Center, Maastricht, the Netherlands
[c] Department of Surgery, University Medical Center Groningen, Groningen, the Netherlands
[d] Department of Biomedical Engineering, Eindhoven University of Technology, Eindhoven, the Netherlands

ARTICLE INFO

Article history:
Accepted 20 May 2019

Keywords:
Peripheral artery disease
Stenosis
Diagnostic method
Angiography
Blood pressure measurement

ABSTRACT

The aim of this study was to develop and verify a model that provides an accurate estimation of the trans-lesion hyperemic pressure gradient in iliac artery stenoses in seconds by only using patient-specific geometric properties obtained from 3-dimensional rotational angiography (3DRA).

Twenty-one patients with symptomatic peripheral arterial disease (PAD), iliac artery stenoses and an ultrasound based peak systolic velocity ratio between 2.5 and 5.0 underwent 3DRA and intra-arterial pressure measurements under hyperemic conditions. For each lesion, geometric properties were extracted from the 3DRA images using quantitative vascular analysis software. Hyperemic blood flow was estimated based on stenosis geometry using an empirical relation. The geometrical properties and hyperemic flow were used to estimate the pressure gradient by means of the geometry-based model. The predicted pressure gradients were compared with *in vivo* measured intra-arterial pressure measurements performed under hyperemic conditions.

The developed geometry-based model showed good agreement with the measured hyperemic pressure gradients resulting in a concordance correlation coefficient of 0.86. The mean bias ± 2SD between the geometry-based model and *in vivo* measurements was comparable to results found by evaluating the actual computational fluid dynamics model (-1.0 ± 14.7 mmHg vs -0.9 ± 12.7 mmHg).

The developed model estimates the trans-lesional pressure gradient in seconds without the need for an additional computational fluid dynamics software package. The results justify further study to assess the potential use of a geometry-based model approach to estimate pressure gradient on non-invasive CTA or MRA, thereby reducing the need for diagnostic angiography in patients suffering from PAD.

1. Introduction

Intermittent claudication is a symptom of peripheral arterial disease caused by one or multiple stenoses. Current clinical guidelines advocate for *in vivo* trans-lesional pressure measurements under hyperemic conditions to discriminate between hemodynamic significant and non-significant stenoses (Norgren et al., 2007). This is especially true in case of equivocal iliac artery stenoses (30%–75% lumen area reduction). Unfortunately, due to the cumbersome nature of invasive pressure measurements and because costs of the expensive pressure monitoring guidewires are often not reimbursed, the majority of experts still do not perform invasive pressure measurements (Heinen et al., 2017a). It could be argued that after acquiring access with a sheath to the common femoral artery, it is easy to advance a fluid-filled catheter (FFC) to the aorta and subsequently measure the pressure gradient over an iliac artery stenosis. However, placing a 4F or 5F FFC through the stenosis results in a significant overestimation of the pressure gradient when compared with a pressure monitoring guidewire (Garcia and Carrozza, 2007).

Recently, various computational fluid dynamics-based computer models have been developed, which are capable to predict the hyperemic pressure gradient (Δp) across iliac (Heinen et al., 2017b) or coronary artery stenoses (Morris et al., 2013; Nkazato et al., 2013; Nørgard et al., 2014). However, because these models take minutes to hours to estimate the pressure gradient and

* Corresponding author at: Koekoekslaan 1, 3430 EM, Nieuwegein, the Netherlands.
E-mail address: s.heinen@antoniusziekenhuis.nl (S.G.H. Heinen).

https://doi.org/10.1016/j.jbiomech.2019.05.030
0021-9290/

because additional computational fluid dynamics software packages are needed to derive the virtual pressure gradient, they are not widely applied yet in clinical practice.

Alternatively, the trans-lesional pressure gradient can be estimated in seconds by using systolic velocity data obtained by duplex ultrasonography (Strauss et al., 1993; Langsfeld et al., 1988) and the Bernoulli approach. Because of its intrinsic assumptions, it might be argued whether the Bernoulli approach is able to accurately predict the pressure gradient across iliac artery stenosis. An accurate, easy applicable and alternative model that could predict the hyperemic pressure gradient (Δp) over (equivocal) iliac artery stenosis would therefore be of great value to physicians.

The aim of this study is to develop and validate a geometry-based model that can instantaneously predict the pressure gradient under hyperemic conditions across common and external iliac artery stenoses while using only geometric input parameters. The diagnostic performance of the geometry-based pressure model is evaluated regarding stenosis severity stratification by comparing the newly developed model to *in vivo* measured pressure gradient under hyperemic conditions.

2. Material and methods

2.1. The geometry-based model

In previous studies Young and Tsai derived a model to describe the pressure gradient caused by flow across an idealized and smooth arterial stenosis while neglecting pressure losses caused by instationary flow effects (Young and Tsai,1973). Their model is given by

$$\Delta p = K_v \frac{8\mu l_s}{\pi a_0{}^3} q + K_t \frac{\rho}{2A_0^2}\left(\frac{A_0}{A_s} - 1\right)^2 q^2 = \Delta p_v + \Delta p_t. \quad (1)$$

The first term on the right-hand side, Δp_v, denotes pressure loss due to viscous forces which is linearly related to the blood flow (q) and Δp_t, the second term on the right-hand side denotes the pressure loss due to convective forces which is quadratically related to the blood flow. These pressure losses depend on the dynamic viscosity ($\mu = 4.5 \cdot 10^{-3}$ kg·m^{-1} s^{-1}), the healthy vessel radius (a_0), the healthy vessel area (A_0), the stenosis area (A_s), the length of the stenosis (ℓ) and the viscous and turbulent loss coefficients, K_v and K_t, respectively. Young and Tsai concluded that the viscous loss coefficient strongly depends on the stenosis geometry and that the turbulent loss coefficient maybe set to 1 (Young and Tsai,1973). However, the turbulent loss coefficient has also been reported to vary with different stenosis severities between 1.81 and 2.06 (Young et al., 1975). Therefore, it was first determined whether the turbulent loss coefficient needs to be defined as function of geometric properties for our application.

To derive the loss coefficients as function of the geometric properties a commonly applied approach that consists of four consecutive steps was used. In the first step, the Buckingham π theorem was applied (Appendix S1) (White, 2011) to relate dimensionless groups to the viscous and turbulent loss coefficients K_v and K_t, respectively. This resulted in $K_v = f(\frac{A_s}{A_0}, \frac{\sqrt{A_0}}{\ell}, \frac{\sqrt{A_s}}{\ell})$ and $K_t = f(\frac{A_s}{A_0}, \frac{\sqrt{A_0}}{\ell}, \frac{\sqrt{A_s}}{\ell})$. The dimensionless groups can easily be acquired e.g. by performing quantitative vascular analysis of computed tomography angiography (CTA), contrast enhanced magnetic resonance angiography (CE-MRA), digital subtraction angiography (DSA) or 3D Rotational Angiography.

In the second step, pressure-flow relations were derived for 1500 unique and independently generated vessel geometries with a parabolically shaped stenosis (Appendix S2). The parabolic shape could easily be defined using the 3 dimensionless parameters from step 1 (Fig. S1). The vessel geometries were generated by quasi-random (Latin hypercube) sampling varying the stenosis length (ℓ; range 0.75 cm to 5 cm), the healthy vessel radius (a_0; range 0.25 cm to 0.75 cm) and the stenosis severity ($S = 1 - \frac{A_s}{A_0}$; range 50% to 95% area reduction). The ranges of the geometric input variables were based on available data of the DETECT-PAD study (Dutch trail registry: NTR5085).

Subsequently, 2D axi-symmetric computer simulations were performed to derive a unique pressure-flow relation over each different parabolically shaped stenosis (Fig. 1A). For the purpose of this study a 2D axi-symmetric model was chosen over a full 3D model because of the following three reasons: (1) in a previous study (Heinen et al., 2017b) it has been shown that the 2D model could accurately describe the pressure-flow relationship over iliac artery stenoses; (2) given the number of 2D simulations required, the use of a 2D model significantly reduces the computational burden; and (3) parametrization of 3D patient-specific geometries is much more difficult than parametrization of a 2D model. A wide range of blood flows was prescribed at the inlet of the generated

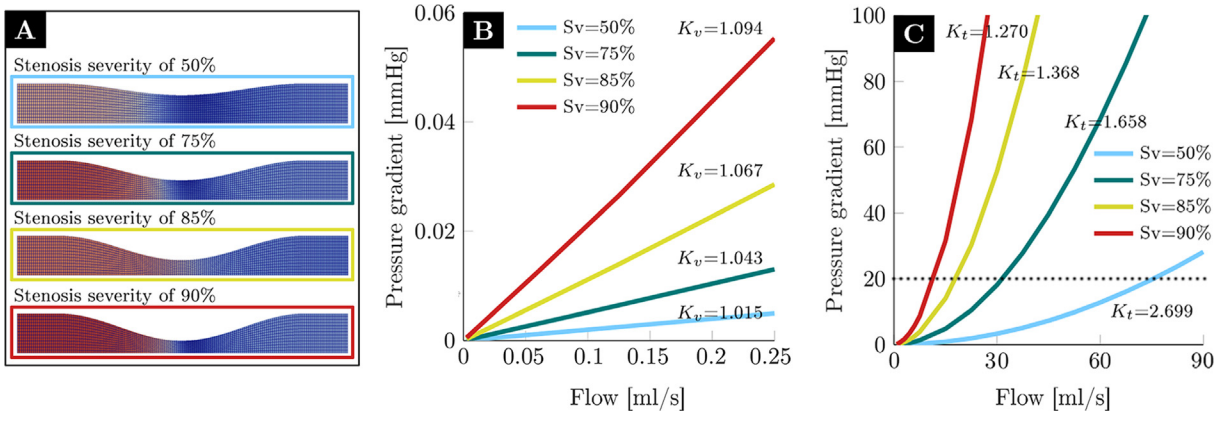

Fig. 1. (A) Four different idealized iliac stenoses geometries with increasing stenosis severity, 50%, 75%, 85% and 90% lumen area reduction were generated (Appendix S2). For each geometry the pressure gradient was calculated for low (B) and high flows (C). At low flows, the flow is dominated by the viscous forces resulting in a linear pressure gradient. At high flows, the flow is dominated by the convective forces resulting in a quadratic pressure gradient. It can be observed that both loss coefficients K_v and K_t are dependent on the vessel geometry. Fore severe stenoses and high Reynolds numbers (i.e. high flows), irrelevant and even unphysiological pressure gradients (e.g. >>50 mmHg) could be found. Therefore only the sample points of the pressure-flow relation that caused a clinically relevant pressure gradient i.e. 0 mmHg < Δp < 20 mmHg, indicated by the dashed line were used to derive K_t.

vessels (Reynolds number (Re) = [0.1–5000]). Because Δp_v and Δp_t were chosen to be independent of time, simulations could be performed using steady inflow (plug profile).

In the third step, K_v and K_t were estimated for each different geometry by fitting the simulated pressure-flow relation (step 2) on Eq. (1). After the third step, the 1500 predictor variables $(\frac{A_s}{A_0}, \frac{\sqrt{A_0}}{\ell}, \frac{\sqrt{A_s}}{\ell})$ with their corresponding K_v and K_t realisations are found. In the fourth and final step a regression model was fitted through the found K_v and K_t realisations as function of the predictor variables. The latter two steps are described in more detail in the next section.

2.2. Approach for deriving the relations for viscous and turbulent loss-coefficients

To estimate the viscous loss coefficient (K_v) for each geometry, it is assumed for the low flow regime (Re < 10) that convective pressure loss (Δp_t) is small compared to the viscous pressure loss (Δp_v) i.e. $\Delta p_v \gg \Delta p_t$. When calculating the analytical friction coefficient at each position across the stenosis (assuming fully developed flow) Eq. (1) reduces to

$$\Delta p \approx \Delta p_v = K_v \frac{8\mu}{\pi {a_0}^4} R_s q, \tag{2}$$

in which $R_s = \int_0^{l_s} \frac{a_0^4}{a^4(z)} dz$. Given the pressure-flow relations obtained in step 2, K_v is the only remaining unknown and can now be estimated for each different geometry. Subsequently, for the high flow regime (Re $\geq$ 10) it can be assumed that the viscous pressure loss (Δp_v) is small compared to the convective pressure loss (Δp_t) i.e. $\Delta p_t \gg \Delta p_v$. Although $\Delta p_t \gg \Delta p_v$, the convective pressure loss (Δp_t) was estimated by

$$\Delta p - \Delta p_v \approx \Delta p_t = K_t \frac{\rho}{2A_0^2} \left(\frac{A_0}{A_s} - 1\right)^2 q^2. \tag{3}$$

Again, using the pressure-flow relations obtained in step 2, the viscous loss coefficient K_t is the only remaining unknown and can be estimated for each different geometry.

Now that K_v and K_t are known, a regression model to fit the derived loss coefficients K_v and K_t as a function of the known predictor variables $\frac{A_s}{A_0}, \frac{\sqrt{A_0}}{\ell}$ and $\frac{\sqrt{A_s}}{\ell}$ was created. Using Matlab software (version R2017b, The Mathworks Inc, Natick, MA, USA) a stepwise regression algorithm was utilized to determine which input parameters significantly contributed to the loss coefficients by iteratively adding and removing predictors (Hocking, 1976). Predictor variables ($\frac{A_s}{A_0}$, $\frac{\sqrt{A_0}}{\ell}$ and $\frac{\sqrt{A_s}}{\ell}$) were added when the adjusted coefficient of determination (R^2-*adjusted*) was improved by at least 0.5% and they were removed when the R^2-*adjusted* decreased by less than 0.25%.

2.3. Clinical data

Patient data from the DETECT-PAD study were used to evaluate the newly developed model. All patients underwent a duplex ultrasound examination, 3DRA with intra-arterial contrast agent injection, and intra-arterial pressure measurements under hyperemic conditions. Quantitative analysis of the 3DRA images showed patients had stenoses with 30%–78% lumen diameter reduction in the common or external iliac artery. An extensive overview of the lesion characteristics is given in Table 1.

2.4. Evaluation of the models

Numerical verification: First, we evaluated whether the use of 2D axi-symmetric simulations alters results with respect to a full 3D model. To that end, a subset of geometries demonstrating clinically relevant pressure gradients (5 mmHg to 15 mmHg) were analysed using a full 3D model. The 3D simulations were performed using FEniCS (http://fenicsproject.org) in combination with the OASIS solver while employing the incremental pressure correction method (Alnæs et al., 2015; Mortensen and Valen-Sendstad, 2015). Time steps of 0.1 ms were found to be sufficiently accurate. Subsequently, it was examined whether the pressure gradient predicted by the derived geometry-based model matched the results of idealized 2D axi-symmetric simulations (Heinen et al., 2017b).

Table 1
Characteristics of twenty-five stenoses. Peak Systolic Velocity (PSV) was measured by duplex ultrasound. Stenoses diameters and lengths were acquired using quantitative vascular analysis software. The hyperemic pressure gradients were simultaneously measured proximally and distally from the lesion after administering 500 μg nitroglycerin. CIA: common iliac artery. EIA: external iliac artery.

Lesion nr.	Blood vessel	PSV [cm/s]	Minimal diameter [mm]	Reference diameter [cm]	Stenosis length [mm]	Hyperemic Δp [mmHg]
#1	CIA	664	2.90	7.88	25.3	43.0
#2	EIA	346	2.86	5.36	23.8	25.7
#3	CIA	494	3.06	9.38	35.0	30.5
#4	CIA	274	4.90	7.50	17.6	5.2
#5	CIA	594	4.78	10.56	13.8	29.2
#6	CIA	418	2.84	6.72	37.5	24.5
#7	CIA	332	5.04	8.22	21.9	8.8
#8	CIA	409	5.88	11.21	42.5	18.5
#9	CIA	626	2.10	9.46	19.8	71.9
#10	CIA	354	5.64	14.32	15.7	7.7
#11	EIA	286	5.64	8.24	13.6	9.8
#12	EIA	345	4.30	7.16	23.7	12.0
#13	EIA	400	4.08	8.7	29.7	13.2
#14	CIA	416	4.56	8.02	15.7	14.3
#15	EIA	243	3.96	6.10	17.8	5.5
#16	CIA	310	3.72	6.76	13.9	13.2
#17	EIA	428	2.54	5.92	19.6	22.5
#18	EIA	485	3.36	8.80	9.8	34.3
#19	CIA	513	3.46	9.44	33.2	21.5
#20	CIA	286	3.28	5.78	9.9	24.0
#21	EIA	107	4.16	7.08	17.8	12.5
#22	EIA	157	3.22	7.08	17.6	23.4
#23	EIA	370	4.40	7.04	31.5	10.8
#24	EIA	332	4.34	6.14	11.8	11.1
#25	CIA	586	2.56	7.62	23.6	40.9

Patient-specific geometries for the models were available from the DETECT-PAD study obtained from 3DRA data (Fig. 2). For the 3D simulations full segmentations were used (Vessel Explorer; Philips Healthcare, Best, The Netherlands). For the 2D simulations, the full 3D segmentation was transformed to a 2D axi-symmetrical mesh using the centre line and radii derived from local cross-sectional areas while assuming circular cross-sections (Heinen et al., 2017). Stenosis severity of the 2D and geometry-based model was evaluated using the maximal distal diameter as a reference. The diameter distal to the stenosis was used to determine the stenosis severity rather than a proximal reference diameter because the pressure losses induced by the stenosis are mainly caused by the expansion of the blood vessel. The hyperemic flow was estimated based on the minimal area of the stenoses using an empirical relation that was derived in a previous study (Heinen et al., 2017b). The agreement between both models was illustrated by drawing a Bland-Altman plot and assessed by calculating the Pearson correlation coefficient (r) and concordance correlation coefficient (ρ_c) with respect to the line $y = x$ (Lin, 1989). The confidence interval (CI) of the ρ_c was given for $\alpha = 0.05$.

Clinical validation: The accuracy of the geometry-based model in predicting pressure gradients patient-specifically was investigated by comparing the predicted pressure gradients with hyperemic *in vivo* measured pressure gradients. A more extensive description of the obtained patient-specific geometries and the *in vivo* pressure measurements can be found in Heinen (Heinen et al., 2017b).

Uncertainty of input parameters should be considered when estimating patient-specific parameters. The input uncertainties of the geometrical parameters (a_0, a_s, ℓ) were estimated based on a phantom study (PIE Medical Imaging, Maastricht, The Netherlands). The healthy vessel area (a_0) could be estimated accurately and the input uncertainty was therefore assumed to be smaller than <±1%. The uncertainty of a_s and ℓ were found to be <±5%. The accuracy of the hyperemic input flow was based on literature and assumed to be <±10% (Lotz et al., 2002). To estimate the uncertainty of the 2D CFD model and the geometry-based model, both models were evaluated 3000 times. Input samples were uniformly distributed and generated using a Latin Hypercube design.

In addition, for patient-specific geometries, the area proximal (A_{prox}) to the stenosis might differ from the area distal (A_{dist}) to the stenosis. To correct for the pressure difference caused by a difference in vessel diameter, the dynamic pressure $-\frac{1}{2}\rho\left(v_{dist}^2 - v_{prox}^2\right)$ was added to the estimated pressure gradient of the geometry-based model. The agreement between the geometry-based model and the *in vivo* measured pressure gradients was subsequently assessed by calculating the ρ_c ($\alpha = 0.05$) with respect to the line $y = x$ and Pearson correlation coefficient (r). This agreement was also illustrated by drawing a Bland-Altman plot.

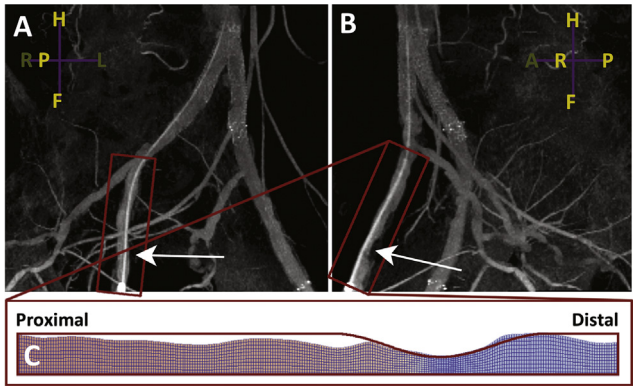

Fig. 2. Examples of patient-specific 2D axi-symmetric meshes as extracted from 3D rotational angiography. A and B, representative 2 orthogonal angiographic projections from the 3-dimensional rotational angiogram, being left-right (A) and anterior-posterior (B). The red frameworks indicate the idealized parabolically shaped geometry (C) that were used to estimate the patient-specific properties for both 2D and the geometry-based model. Idealized stenosis geometries were fitted on the distal reference diameter, because the pressure losses induced by the stenosis are mainly caused by the expansion of the blood vessel. (For interpretation of the references to colour in this figure legend, the reader is referred to the web version of this article.)

To assess the diagnostic value of the geometry-based model, the pressure gradients calculated by the geometry-based model were stratified into three groups. Model predictions were categorized as hemodynamic non-significant if the upper bound of the uncertainty interval of the predicted trans-lesional pressure gradient was <10 mmHg or as hemodynamic significant when the lower bound of the uncertainty interval of the predicted trans-lesional pressure gradient was ≥10 mmHg (Klein et al., 2006). The model prediction was considered doubtful when the uncertainty of the predicted pressure gradient overlapped with the treatment threshold of 10 mmHg. The *in vivo* measured pressure gradients were stratified into two groups either indicating a hemodynamic non-significant stenosis (<10 mmHg) or a hemodynamic significant stenosis (≥10 mmHg). The diagnostic value was assessed by determining the sensitivity, specificity and overall accuracy. The 95% confidence interval of these diagnostic parameters was estimated using a scoring method incorporating continuity correction (Newcombe, 1998).

Added value of the geometry-based model: To investigate the potential added value of the geometry-based model, the performance of the Bernoulli approach (Eqs. (4) and (5)) was also investigated. The maximal systolic velocity (v_{max}[m/s]) and proximal systolic velocity (v_{prox}[m/s]) which serves as a reference were obtained using duplex ultrasonography at rest as is done in everyday clinical practice (Heinen et al., 2018). The obtained velocity data is then inserted in the following equation:

$$\Delta p = \frac{1}{2}\rho(v_{max}^2 - v_{prox}^2). \tag{4}$$

with $\rho = 1050$ kg/m^3 (blood density) and the pressure gradient (Δp) in Pascal. Eq. (4) is in clinical practice often further simplified by assuming that the maximal velocity is much higher than the proximal velocity. This assumption reduces Eq. (4) after conversion from the unit Pascal to mmHg in:

$$\Delta p \approx 4 v_{max}^2. \tag{5}$$

The pressure gradients estimated by Bernoulli approach were correlated with the *in vivo* measured pressure gradients by calculating the Pearson correlation coefficient (r) and the concordance correlation coefficient ($\rho_c, \alpha = 0.05$) with respect to the line $y = x$ and the agreement was illustrated by drawing a Bland-Altman plot.

3. Results

3.1. Deriving K_v and K_t

Fifteen hundred vessel geometries (Appendix S2) were successfully generated which is a sufficient sample size for an excellent prediction of the regression coefficients of the regression models to fit K_v and K_t (Knofczynski and Mundfrom, 2007). Using the stepwise regression model the viscous loss-coefficient was found to depend significantly on two geometric parameters i.e. $\frac{\sqrt{A_0}}{\ell}$ and $\frac{\sqrt{A_s}}{\ell}$. Adding the $\frac{A_s}{A_0}$ did not significantly improve the R^2-*adjusted*. When fitting the regression model as function of the two significant dimensionless groups a regression model with an excellent

R^2-*adjusted* (>0.99) was obtained (Fig. 3). The regression model was found to be

$$K_v\left(\frac{\sqrt{A_0}}{\ell},\frac{\sqrt{A_s}}{\ell}\right)=a_0+a_1\frac{\sqrt{A_0}}{\ell}+a_{11}\frac{A_0}{\ell^2}+a_2\frac{\sqrt{A_s}}{\ell}+a_{22}\frac{A_s}{\ell^2}. \quad (6)$$

The estimated regression coefficients $a_0, a_1,$ etc. are shown in Table 2. Subsequently, loss coefficient K_t was fitted on the same data by means of a least square fit. The turbulent loss coefficient significantly depends on the stenosis severity and $\frac{\sqrt{A_0}}{\ell}$. Fitting K_t as function of these two geometric parameters also resulted in an excellent R^2-*adjusted* (>0.98) (Fig. 3). Using the stepwise regression model the turbulent loss-coefficient could be defined as a function of the $\frac{A_s}{A_0}$ and $\frac{\sqrt{A_0}}{\ell}$ i.e.

$$K_t\left(\frac{A_s}{A_0},\frac{\sqrt{A_0}}{\ell}\right)=b_0+b_1\frac{\sqrt{A_0}}{\ell}+b_2\frac{A_s}{A_0}+b_{22}\frac{A_s^2}{A_0^2} \quad (7)$$

Estimated coefficients are shown in Table 2.

3.2. Verification of the geometry-based model

Numerical verification: Within the subset of geometries demonstrating clinically relevant pressure gradients (5 mmHg to 15 mmHg) that were evaluated both with a full 3D model and a 2D axi-symmetrical model, the estimated pressure gradients were on average slightly higher for the 3D model (median 2.4 mmHg, range −2.7 mmHg – 3.2 mmHg; Fig. 4). The 2D axi-symmetrical model was therefore considered sufficiently accurate to derive the geometry-based model. The pressure gradients calculated over patient-specific geometries as calculated by the geometry-based model were compared to the pressure gradients calculated by the 2D axi-symmetric mode. The concordance correlation coefficient between the geometry-based model and 2D model with respect to the line y = x (Fig. 5A) was 0.99 (CI 0.97–0.99) and the Pearson correlation was 0.99, demonstrating excellent agreement. The differences between the pressure gradient predicted by the geometry-based and 2D model were normally distributed ($p = 0.38$). The mean bias between the geometry-based model and 2D model was 0.6 ± 4.1 mmHg (mean ± 2SD), which can be seen in the Bland-Altman plot (Fig. 5B). The use of $K_v = \left(\frac{A_0}{A_s}\right)^2$ and $K_t = 1$, as proposed by Young and Tsai (1973) resulted in an underestimation of the actual hyperemic pressure gradient by −8.0 ± 6.3 mmHg (mean ± 2SD), with a Pearson correlation of $r = 0.98$ and a ρ_c of 0.76 (CI 0.63–0.86).

Table 2
Coefficients of the fitted regression models for estimating the viscous (K_v) (Eq. (6)) and turbulent loss coefficient (K_t) (Eq. (7)).

Coefficients	Value
a_0	0.98
a_1	0.27
a_{11}	0.34
a_2	−0.28
a_{22}	−0.45
b_0	6.04
b_1	0.21
b_2	−8.65
b_{22}	3.66

Clinical validation: For each lesion the hyperemic pressure gradient as calculated using the derived geometry-based model was compared to the *in vivo* measured hyperemic pressure gradient. The concordance correlation coefficient (ρ_c) between the geometry-based model and *in vivo* measured pressure gradients with respect to the line y = x (Fig. 6A) was 0.86 (CI 0.71–0.93) and the Pearson correlation was 0.87. The differences between the pressure gradient predicted by the geometry-based and *in vivo* were normally distributed ($p = 0.57$). The mean bias between the geometry-based model and *in vivo* measurements was −1.0 ± 14.7 mmHg (mean ± 2SD), which can be seen in the Bland-Altman plot (Fig. 6B). These results were comparable to results found with the actual 2D CFD model (−0.9 ± 12.7 mmHg) (Fig. 4) (Heinen et al., 2017b). The model of Young and Tsai (1973) again resulted in an underestimation of the actual hyperemic pressure gradient by −9.6 ± 14.2 mmHg (mean ± 2SD) with a Pearson correlation of $r = 0.90$ and a ρ_c of 0.66 (CI 0.47–0.79).

Subsequently, the pressure gradients derived from the geometry-based model and *in vivo* measured pressure gradients

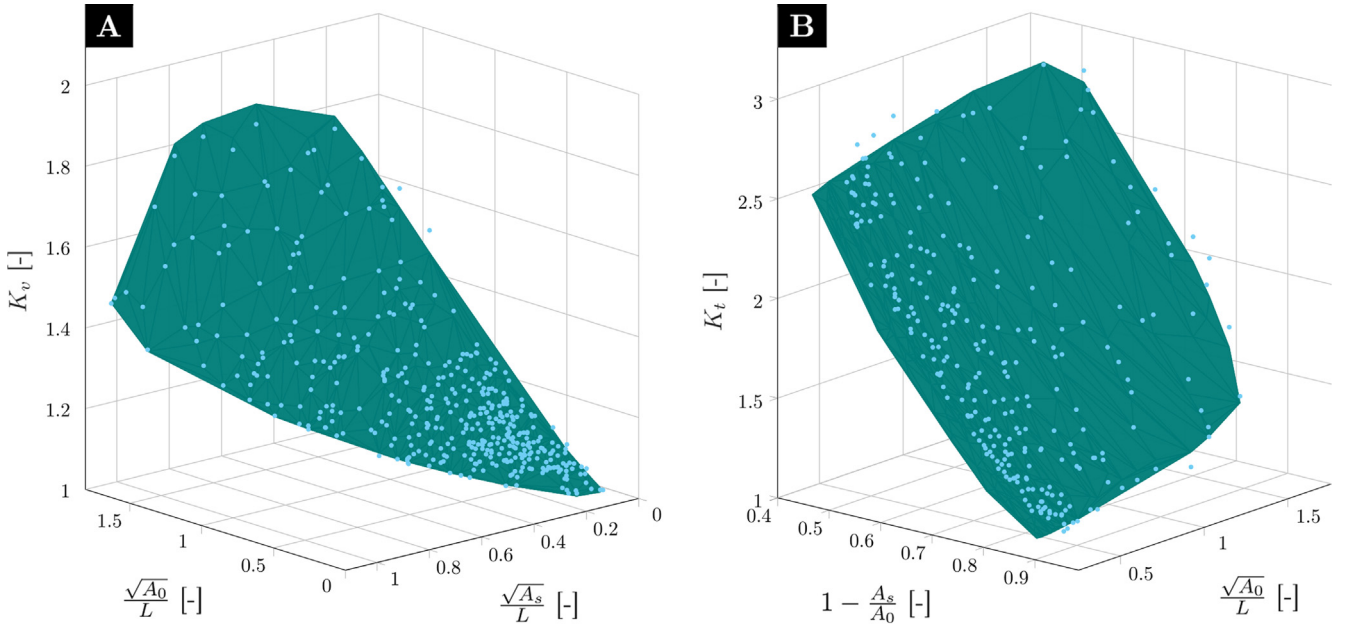

Fig. 3. (A) The viscous loss coefficient (K_v) fitted as a function of $\frac{\sqrt{A_0}}{\ell}$ and $\frac{\sqrt{A_s}}{\ell}$. (B) The turbulent loss coefficient (K_t) fitted as function of the $\frac{A_s}{A_0}$ and $\frac{\sqrt{A_0}}{\ell}$. The coefficients were estimated by means of a least square fit using a stepwise regression approach.

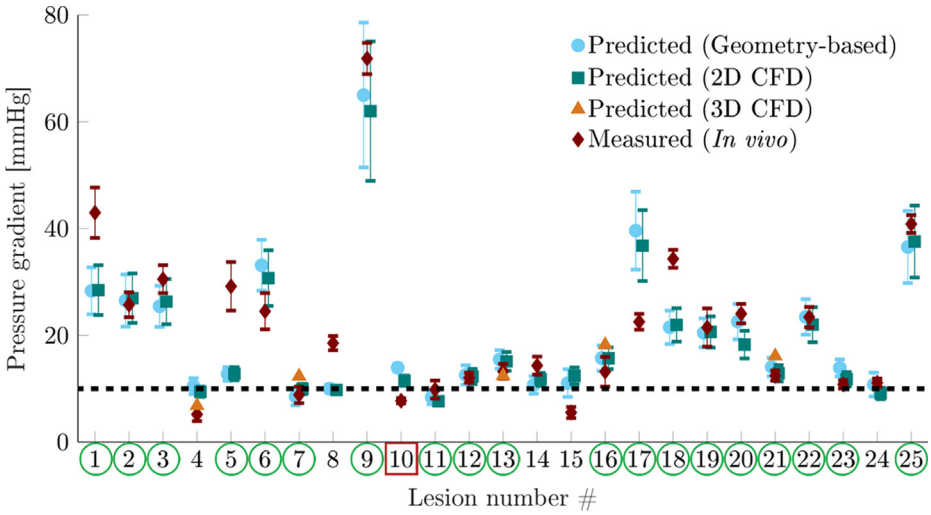

Fig. 4. Predicted pressure gradient by the geometry-based model (blue), 2D CFD model (green), and 3D CFD model (orange) as well as, *in vivo* measured pressure gradient observed after administering of a vasoactive drug (red). Only a minimal difference between the results of the 2D and 3D CFD model was observed. The results of the 2D CFD model and geometry-based model show good agreement. The uncertainty on the prediction is given by 2SD. The black dashed line indicates the clinically applied cut-off for hemodynamic significant stenoses ($\Delta p \geq 10$ mmHg). A green circle around a lesion indicates a correct prediction of the geometry-based model. A red square indicates an erroneous prediction of the geometry-based model. For the remainder of the stenoses, the geometry-based model prediction was considered doubtful. For these stenoses it would be advised to measure the pressure gradient invasively. (For interpretation of the references to colour in this figure legend, the reader is referred to the web version of this article.)

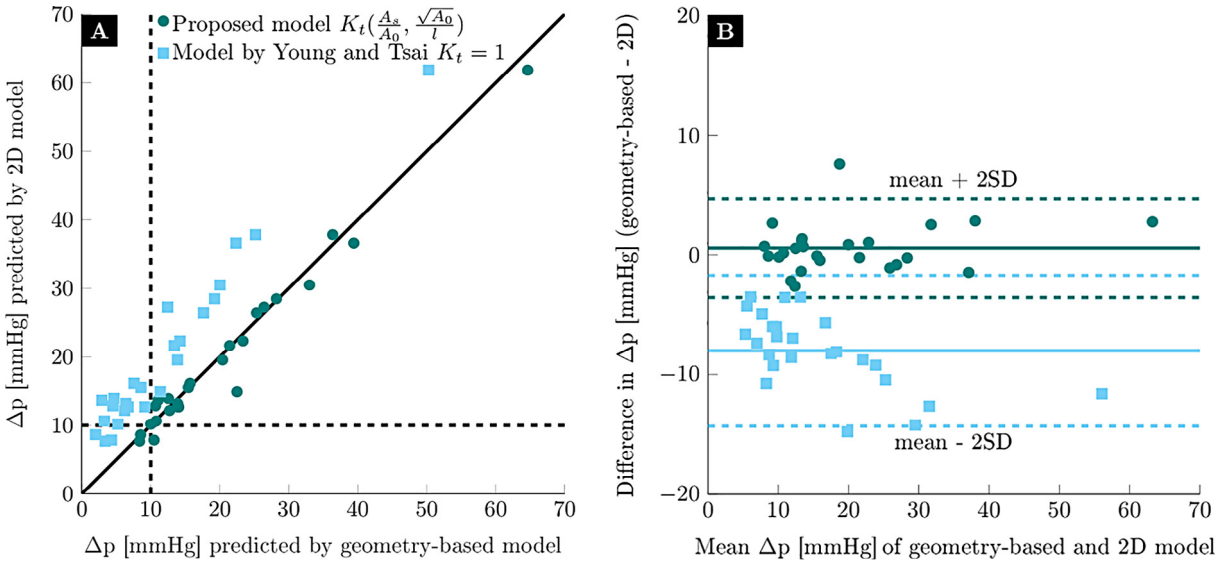

Fig. 5. (A) The hyperemic pressure gradient calculated by the 2D axi-symmetric model plotted against the proposed geometry-based model ($K_t(\frac{A_s}{A_0}, \frac{\sqrt{A_0}}{l})$) shown in green and the model of Young and Tsai ($K_t = 1$) shown in blue. The concordance correlation coefficient for the proposed model and the model of Young and Tsai were 0.97 and 0.29 respectively. (B) Bland-Altman plot for the pairwise comparison between the geometry-based models and the 2D axi-symmetric model. The mean bias of the proposed model was 0.6 ± 4.1 mmHg (mean ± 2SD) whereas the model of Young and Tsai resulted in an underestimation (−8.0 ± 6.3 mmHg). (For interpretation of the references to colour in this figure legend, the reader is referred to the web version of this article.)

were stratified into three groups (hemodynamic non-significant, doubtful, or hemodynamic significant) with 10 mmHg as a cut-off value. The uncertainty interval of the predicted pressure gradient of five stenoses overlapped with the clinical cut-off value of 10 mmHg. These predictions were therefore classified as doubtful model prediction (Table 3). For the 20 stenoses which had no overlapping uncertainty interval with the clinical threshold value, the geometry-based model draws the same conclusion as the *in vivo* measured pressure gradients in 19 of 20 lesions. This resulted in 100% (CI 80.0%–100%) sensitivity, 67% (CI 42.5%–85.5%) specificity and 95% (CI 73.1%–100%) overall diagnostic accuracy.

Added value of the geometry-based model: The pressure gradients calculated by the Bernoulli approach using velocities obtained at rest were compared to *in vivo* measured pressure gradients under hyperemic conditions. Although, velocities at rest were used, the Bernoulli approach strongly overestimated the *in vivo* measured hyperemic pressure gradient (Fig. 7A). The mean bias between the Bernoulli approach and *in vivo* measurements was 47.7 ± 67.4 mmHg (mean ± 2SD), which is shown in the Bland-Altman plot (Fig. 7B). The concordance correlation coefficient (ρ_c) was 0.18 (CI 0.09–0.27) and the Pearson correlation was 0.80. Taken into account the maximal proximal reference velocity and applying $\Delta p \approx 4(v_{max}^2 - v_{prox}^2)$ instead of $\Delta p \approx 4v_{max}^2$ slightly improved the results (41.2 ± 68.5 mmHg, ρ_c = (0.21, CI 0.11–0.31, r = 0.82) but still resulted in a significantly overestimated pressure gradient.

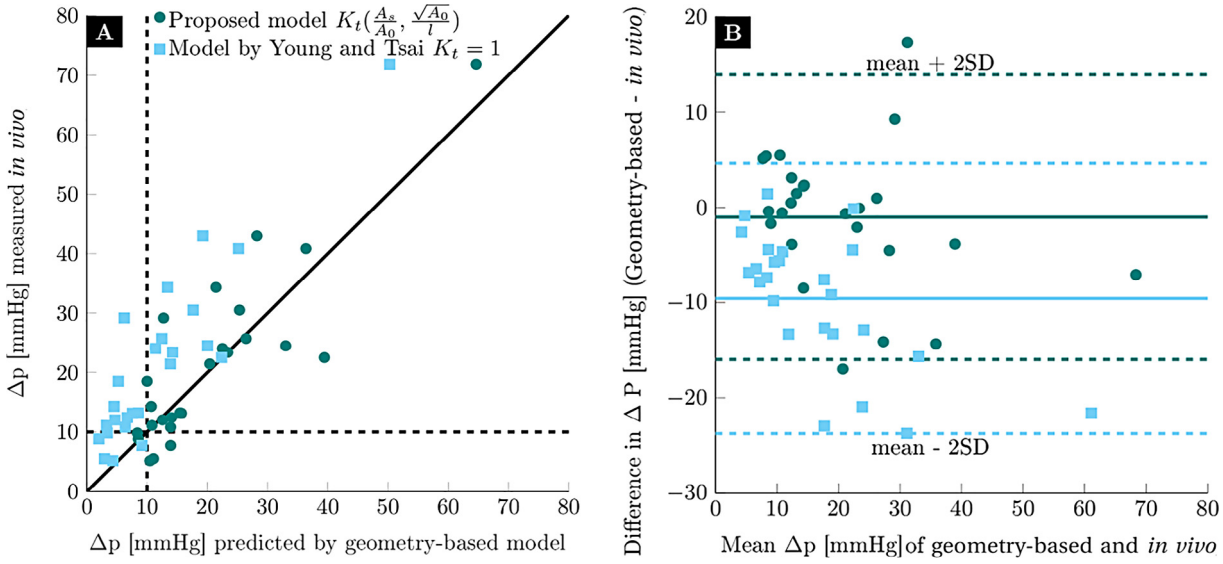

Fig. 6. (A) The *in vivo* measured hyperemic pressure gradient plotted against the proposed geometry-based model ($K_t(\frac{A_s}{A_0}, \frac{\sqrt{A_0}}{l})$) shown in green and the model of Young and Tsai ($K_t = 1$) shown in blue. The concordance correlation coefficient for the proposed model and the model of Young and Tsai were 0.66 and −0.35 respectively. (B) Bland-Altman plot for the pairwise comparison between the geometry-based models and the *in vivo* measured hyperemic pressure gradient. The mean bias of the proposed model was −1.0 ± 14.7 mmHg (mean ± 2SD) whereas the model of Young and Tsai resulted in an underestimation (−9.6 ± 14.2 mmHg). (For interpretation of the references to colour in this figure legend, the reader is referred to the web version of this article.)

Table 3
Number of significant stenoses as identified by the geometry-based model with *in vivo* measured pressure gradients as a reference. Model predictions were categorized as hemodynamic non-significant if the upper boundary of the uncertianty interval of the predicted trans-lesional pressure gradient was <10 mmHg or as hemodynamic significant when the lower boundary of the uncertainty interval of the predicted trans-lesional pressure gradient was ≥10 mmHg. The model prediction was considered doubtful when the uncertainty of the predicted pressure gradient overlapped with the treatment threshold of 10 mmHg.

	Measured pressure gradient		
	Δp < 10 mmHg	Δp ≥ 10 mmHg	Total
Predicted			
Δp < 10 mmHg	2	0	2
Doubtful	2	3	5
Δp ≥ 10 mmHg	1	17	18
Total	5	20	25

4. Discussion

The aim of this study was to develop and validate a geometry-based model that instantaneously predicts the pressure gradient across common and external iliac artery stenoses under hyperemic conditions without the need for an additional computational fluid dynamics software package. The model is developed based on physical insights with input parameters that can directly be derived from angiographic images. From the performed computer simulations it was concluded that the turbulent loss coefficient (K_t) strongly depends on the severity of the iliac artery stenosis. If pressure gradients were estimated with a fixed $K_t = 1$ as proposed by Young and Tsai, the linear correlation between estimated and actual hyperemic pressure gradient was good but strongly underestimated the actual hyperemic pressure gradient. Defining K_t as a function of the stenosis geometry rather than using a fixed value reduces bias and is a strong improvement to the original model by Young and Tsai.

Our model is validated with *in vivo* measured intra-arterial pressure gradients under hyperemic conditions. In line with Gashi et al. (2019), who already demonstrated that for application of modelling the pressure gradients across coronary artery stenoses a 3D steady model could be replaced with computationally less expensive models such as a 2D axi-symmetrical model, we first showed that this simplified approach can also be used in case of common iliac artery stenoses (Fig. 4). Hence we were confident that the 2D axi-symmetrical model was sufficiently accurate to derive the geometry-based model that on its turn showed good agreement with respect to the *in vivo* measured pressure gradient ($\rho_c = 0.86$, $r = 0.87$). Results (mean ± 2SD) of the geometry-based model were comparable to the results of the actual 2D CFD model. Overlap between the uncertainty interval of the pressure drop predicted by the geometry-based model and the clinical cut-off value of 10 mmHg was observed in five of twenty-five lesions (20%). These five predictions were classified as doubtful predictions. It would therefore be recommended to measure the actual *in vivo* pressure drop. For the remaining 20 stenoses, which had no overlapping uncertainty interval with the clinical threshold value, the geometry-based model could discriminate between hemodynamically significant and non-significant lesions with 95% accuracy. This accuracy is higher than the ones of peak systolic velocity ratios measured by duplex ultrasonography (77%–81%) (Legemate et al., 1991; Heinen et al., 2018) and geometry-based diagnosis on the basis of visual inspection of digital subtraction angiographies (71%–81%) (Breslau et al., 1985; Legemate et al., 1991). Our newly developed approach significantly improved the estimate of the pressure gradient by reducing mean bias and standard deviation, and in addition it improved the ρ_c compared to the Bernoulli approach. Although the Bernoulli approach was evaluated using velocity measurements at rest, the pressure gradient was still largely overestimated and poorly correlated with the actual *in vivo* measured pressure gradient under hyperemic conditions. The derived geometry-based model as presented in this article offers a simple and more accurate method to estimate the hemodynamic significance of an iliac artery stenosis under hyperemic conditions while it only uses geometric properties that can be obtained at rest.

Despite good correlations (0.78–0.9) between the Bernoulli approach and intra-arterial pressure gradients, it was already observed in the late eighties and early nineties that the Bernoulli approach results in overestimation of the pressure gradient

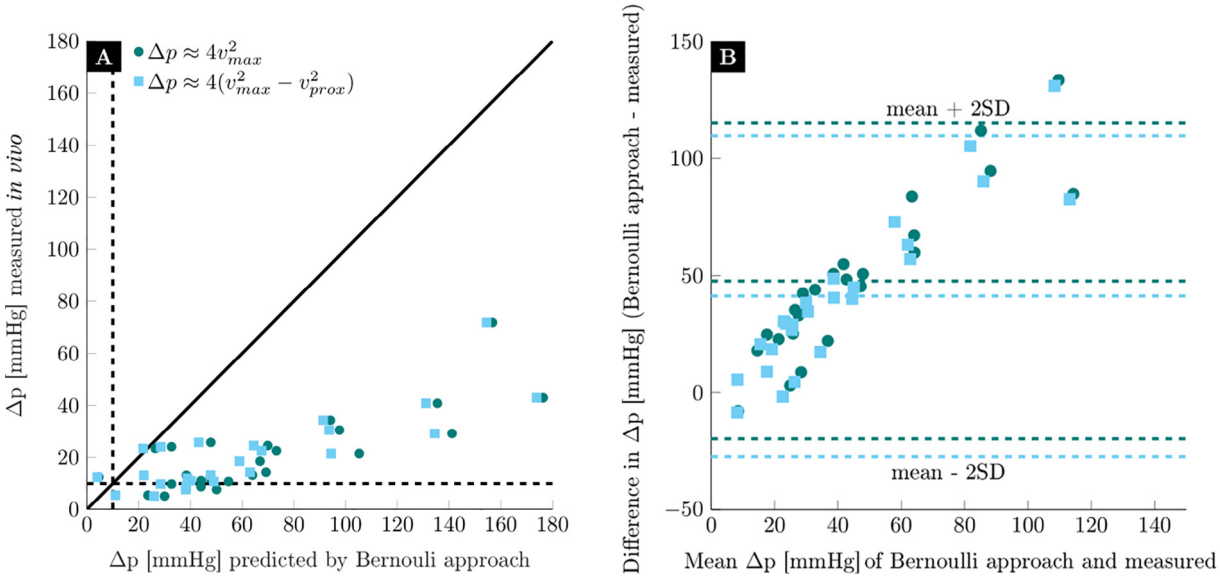

Fig. 7. (A) A comparison between the pressure gradients calculated between both Bernoulli approaches and the *in vivo* measured hyperemic pressure gradient. The concordance correlation coefficient of −0.77 and −0.43 were demonstrating poor agreement. (B) A very strong overestimation can be observed from the Bland-Altman plot for the pairwise comparison between both Bernoulli equations and the actual *in vivo* hyperemic pressure gradient. The mean bias between $\Delta p = 4v^2_{max}$ (green) and the *in vivo* measured hypermic pressure gradient was 47.7 ± 67.7 mmHg (mean ± 2SD). The mean bias between $4(v^2_{max} - v^2_{prox})$ (blue) and the *in vivo* measured hyperemic pressure gradient was 41.2 ± 68.5 mmHg (mean ± 2SD). (For interpretation of the references to colour in this figure legend, the reader is referred to the web version of this article.)

(Kohler et al.,1987; Langsfeld et al., 1988). The degree of overestimation was found to be related to the stenotic diameter, being largest for diameters smaller than 4 mm which is typically the case for iliac artery stenoses (Giardini and Tacy, 2010). Because of the overestimation present, application of the Bernoulli approach to estimate the hemodynamic significance of iliac artery stenosis in everyday clinical practice should be done with caution (Giardini and Tacy, 2010).

A disadvantage of our approach is that the geometry-based model was tested on 3DRA data which is not common practice in the diagnostic workflow of most hospitals and has to be acquired in the cath lab. To assess stenosis severity before the patient enters the cath lab, the proposed approach could also be applied using pre-procedural geometric information e.g. CTA and CE-MRA. Alternatively, the geometric information of two or three 2D angiographic acquisitions could be combined and used to estimate the hyperemic pressure gradient.

Although patients were selected on the basis of equivocal stenoses (duplex ultrasonography, 50%–75% diameter reduction), the number of lesions with a hyperemic trans-lesional pressure gradient around the clinical threshold value (5 mmHg–15 mmHg) is limited (N = 12). Because these lesions cause most doubt regarding the need for revascularization, a larger number of lesions around the clinical threshold need to be included to determine the true diagnostic value of the geometry-based model.

The geometry-based model could possibly be further improved by fitting the viscous and turbulent loss coefficient using full 3D CFD simulations. This would also open the opportunity for the incorporation of a larger number of geometric parameters, thereby possible contributing to a more accurate description of the pressure gradient across an iliac artery stenosis. However, note that geometric parameterization is more challenging in full 3D. Other future directions for research could be to investigate the influence of curvature and eccentricity by performing full 3D simulations for all patients and to investigate whether the presence of a second stenosis in the same artery (tandem lesion) can be described by adding additional geometric parameters.

5. Conclusion

In this study a geometry-based model for which input can directly be obtained from 3D rotational angiography, was derived and validated against *in vivo* measured pressure gradients. The geometry-based model can easily be applied without the need for an additional CFD software package and help to select those lesions that are the hardest to diagnose and warrant *in vivo* measurements using expensive pressure-monitoring guidewires.

Declaration of Competing Interest

As the corresponding author of this article, I hereby declare that there has been no conflict of interest of any of the authors, all authors have read and approved the manuscript, there has been no duplicate publication or submission of any of the work and there are no commercial affiliations or consultations.

Acknowledgements

We sincerely thank M.H.A. van den Elzen for performing the 3D computer simulations

Sources of funding

St. Antonius Research fund, unrestricted grant by Volcano Inc., and the Dutch Endovascular Alliance.

Appendix A. Supplementary material

Supplementary data to this article can be found online at https://doi.org/10.1016/j.jbiomech.2019.05.030.

References

Alnæs, M., Blechta, J., Hake, J., Johansson, A., Kehlet, B., Logg, A., Richardson, C., Ring, J., Rognes, M.E., Wells, G.N., 2015. The fenics project version 1.5. Arch. Numer. Softw. 3, 9–23.

Breslau, P.J., Jörning, P.J., Greep, J.M., 1985. Assessment of aortoiliac disease using hemodynamic measures. Arch. Surg. 120, 1050–1052.

Gashi, K., Bosboom, E.M.H., Van de Vosse, F.N., 2019. The influence of model order reduction on the computed fractional flow reserve using parameterized coronary geometries. J. Biomech. 82, 313–323.

Garcia, L.A., Carrozza Jr, J.P., 2007. Physiologic evaluation of translesion pressure gradients in peripheral arteries: comparison of pressure wire and catheter-derived measurements. J. Interv. Cardiol. 20, 63–65.

Giardini, A., Tacy, T.A., 2010. Pressure recovery explains doppler overestimation of invasive pressure gradient across segmental vascular stenosis. Echocardiography 27, 21–31.

Heinen, S.G.H., de Boer, S.W., van den Heuvel, D.A.F., et al., 2018. Hemodynamic significance assessment of equivocal iliac artery stenoses by comparing duplex ultrasonography with intra-arterial pressure measurements. J. Cardiovasc. Surg. (Torino) 59, 37–44.

Heinen, S.G.H., de Boer, S.W., van den Heuvel, D.A.F., et al., 2017a. How to define the hemodynamic significance of an equivocal iliofemoral artery stenosis: review of literature and outcomes of an international questionnaire. Vascular 25, 598–608.

Heinen, S.G.H., van den Heuvel, D.A.F., Huberts, W., et al., 2017b. In vivo validation of patient-specific pressure gradient calculations for iliac artery stenosis severity assessment. J. Am. Heart Assoc. 6. https://doi.org/10.1161/JAHA.117.007328.

Hocking, R.R., 1976. The Analysis and Selection of Variables in Linear Regression. Biometrics 32, 1–49.

Klein, W.M., van der Graaf, Y., Seegers, J., et al., 2006. Dutch iliac stent trial: long-term results in patients randomized for primary or selective stent placement. Radiology 238, 734–744.

Knofczynski, G., Mundfrom, D., 2007. Sample sizes when using multiple linear regression for prediction. Educ. Psychol. Measur. 68, 431–442.

Kohler, T.R., Nicholls, S.C., Zierler, R.E., et al., 1987. Assessment of pressure gradient by Doppler ultrasound: experimental and clinical observations. J. Vasc. Surg. 6, 460–469.

Langsfeld, M., Nepute, J., Hershey, F.B., et al., 1988. The use of deep duplex scanning to predict hemodynamically significant aortoiliac stenoses. J. Vasc. Surg. 7 (395–399), 1991.

Legemate, D.A., Teeuwen, C., Hoeneveld, H., Eikelboom, B.C., 1991. Value of duplex scanning compared with angiography and pressure measurement in the assessment of aortoiliac arterial lesions. Br J Surg 78, 1003–1008.

Lin, L.I.K., Concordance, A., 1989. Correlation coefficient to evaluate reproducability. Biometrics 45, 255–268. https://www.ncbi.nlm.nih.gov/pubmed/2720055.

Lotz, J., Meier, C., Leppert, A., Glanski, M., 2002. Cardiovascular flow measurements with phase-contrast MR Imaging: Basic facts and implementation. Radiographics 22, 651–671. https://www.ncbi.nlm.nih.gov/pubmed/12006694.

Morris, P.D., Ryan, D., Morton, A.C., et al., 2013. Virtual fractional flow reserve from coronary angiography: modeling the significance of coronary lesions: results from the VIRTU-1 (VIRTUal fractional flow reserve from coronary angiography) study. JACC Cardiovasc. Interv., 149–157

Mortensen, M., Valen-Sendstad, K., 2015. Oasis: a high-level/high-performance open source Navier-Stokes solver. Comput. Phys. Commun. 188, 177–188.

Nakazato, R., Park, H.B., Berman, D.S., et al., 2013. Noninvasive fractional flow reserve derived from computed tomography angiography for coronary lesions of intermediate stenosis severity: results from the DeFACTO study. Circ. Cardiovasc. Imaging, 881–889.

Newcombe, R.G., 1998. Two-sided confidence intervals for the single proportion: comparison of seven methods. Stat. Med. 17, 857–872.

Nørgaard, B.L., Leipsic, J., Gaur, S., et al., 2014. On behalf of the NXT Trial Study Group. Diagnostic performance of noninvasive fractional flow reserve derived from coronary computed tomography angiography in suspected coronary artery disease. J. Am. Coll. Cardio., 1145–1155

Norgren, L., Hiatt, W.R., Dormandy, J.A., et al., 2007. Inter-society consensus for the management of peripheral arterial disease. Int. Angiol. 26, 81–157.

Strauss, A.L., Roth, F.J., Rieger, H., 1993. Noninvasive assessment of pressure gradients across iliac artery stenoses: duplex and catheter correlative study. J. Ultrasound Med. 12, 17–22.

White, F., 2011. Fluid Mechanics. McGraw-Hill Book Company, New York, pp. 293–306.

Young, D.F., Cholvin, N.R., Roth, A.C., 1975. Pressure drop across artificially induced stenoses in the femoral arteries of dogs. Circ. Res. 36, 735–743.

Young, D.F., Tsai, F.Y., 1973. Flow characteristics in models of arterial stenoses. I. Steady flow. J. Biomech. 6, 395–410.